Journal of Intelligent & Robotic Systems (2024) 110:71
https://doi.org/10.1007/s10846-024-02102-6

REGULAR PAPER

A Soft Supernumerary Robotic Limb with Fiber-Reinforced Actuators

Jiajun Xu[1] · Tianyi Zhang[1] · Kaizhen Huang[1] · Mengcheng Zhao[1] · Xuyan Hou[2] · Youfu Li[3]

Received: 6 December 2023 / Accepted: 18 April 2024

Abstract
Supernumerary robotic limbs (SRLs) have great potentials to assist human in daily activities and industrial manufacturing by providing extra limbs. However, current SRLs have heavy and rigid structures that may threaten the operator safety; moreover, their limited degrees of freedom and movement modes are not suitable for complicated tasks. Although soft SRLs have exhibited advantages in structure compliance and flexible manipulation to address these problems, it remains challenging to accurately design the geometrical parameters to adapt to specific tasks, and accurate control is also required to realize the expected movement. Inspired by the biological characteristics of the octopus arm muscle fibers, fiber-reinforced actuators (FRAs) are employed to realize various motions, including extension, expansion, bending, and twisting; multiple FRAs are assembled to implement the SRL to achieve complex movement trajectories. The analytic model of the FRA is established to reveal the relationship between its deformation and geometrical parameters as well as input air pressures, which is validated with finite element simulation. Trajectory and payload optimization algorithms are proposed to optimally design the SRL and its control strategy with meeting the prescribed requirement of movement trajectory and payload capacity. Finally, experiments are conducted to validate the proposed robotic system.

Keywords Supernumerary robotic limb · Fiber-reinforced actuator · Design and fabrication · Finite element method · Trajectory optimization · Payload optimization

1 Introduction

Supernumerary robotic limbs (SRLs) are a new type of wearable auxiliary equipment to perform as an extra leg or arm for the operator [1]. SRLs have broad applications in many fields like daily activities and industrial manufacturing. A pair of robotic manipulators are used brace an aircraft assembly worker body and guide the wearer's hands by placing a drill jig on the aircraft structure surface for drilling assistance [2]. A SuperLimb is developed to assist with the operator to accomplish overhand tasks by providing necessary supporting forces on overhand objects, such that his/her both hands are available for complex operation [3]. While the operator works near floor level in an uncomfortable posture, the braced SRL can support on the ground to keep balance and reduce load on human body [4]. A SRL powered by magnetorheological actuators can assist human in walking and completing various teleoperation, such as vegetables picking, painting on a wall, and washing a window [5, 6]. The current mainstream research on SRLs primarily employs rigid structures with motors and tendons as the driving units. Although the benefits from using SRLs are evident, current SRLs are mostly

✉ Jiajun Xu
xujiajun@nuaa.edu.cn

Tianyi Zhang
zhangtianyi096@nuaa.edu.cn

Kaizhen Huang
huangkaizhen@nuaa.edu.cn

Mengcheng Zhao
zhaomengcheng@nuaa.edu.cn

Xuyan Hou
houxuyan@hit.edu.cn

Youfu Li
meyfli@cityu.edu.hk

[1] College of Mechanical and Electrical Engineering, Nanjing University of Aeronautics and Astronautics, 29 Yudao Street, Najing, Jiangsu Province, China

[2] School of Mechatronics Engineering, Harbin Institute of Technology, Harbin, China

[3] Department of Mechanical Engineering, City University of Hong Kong, Hong Kong, China

Published online: 10 May 2024

composed of heavy and rigid structures, and it is unavoidable for them to interact with obstacle objects and human bodies, decreasing the wearing comfort and even threatening the operator safety. Moreover, the limited motion flexibility and degree-of-freedom categories (only translation and rotation) of traditional SRLs are inadequate to handle with complex manipulation tasks, especially in three-dimensional space.

One potential solution to tackle these challenges originates from soft robotics. Generally, soft robots have the advantages of lightweight structure, high power-to-weight ratios, great adaptability to changing environment and compliant human–robot interaction, exactly compensating for the limitations of traditional rigid SRLs [7]. The blend of soft robotics and SRL sets forth the emergence of soft SRLs, but the research of soft SRLs has just begun with limited outcomes. A Soft Poly-Limb is developed using modular ring-reinforced actuators, and it is capable of three-dimensional motion in space [8]. Each actuator extends axially when pressurized, and the contact interactions between the actuators induce spatial bending motion of the SRL. Subsequently, a SRL implemented with high-strength inflatable fabrics demonstrates increasing payload capacity [9, 10]. Thermoplastic polyurethane actuators encased in nylon fabric casings constitute bending actuator array, and it can generate vertical and horizontal bending motion when inflated. Obviously, the compliant nature of soft SRLs allows comfortable wearing experience, and their manipulation flexibility achieves better effects than rigid SRLs. Nonetheless, the drawbacks of current soft SRLs lies in that the existing actuation methods can only generate monotonous motion mode, not capable of accomplishing complicated manipulation tasks. Soft SRLs typically consist of soft materials, which exhibit nonlinear relationship between the driving position/force and their influencing parameters. The lack of theoretical model that quantitatively analyzes the deformation regulation hinders the accurate control of the soft SRLs. Therefore, a novel soft SRL that can realize complex and controllable motions is required to address the abovementioned drawbacks.

Creatures in nature have inspired us much to improve robot design. For example, octopus arms can realize various motions due to the biological characteristics of the muscular hydrostat, where different classifications of muscle fibers are arranged. Specifically, transverse, longitudinal and oblique muscle fibers are distributed in different locations and orientations, and they function cooperatively to move in arbitrary direction in three-dimensional space [11, 26]. By mimicking the muscle fibers of octopus tentacles, fiber-reinforced actuators with changing fiber angles can produce different motions, including axial extension, radial expansion, bending, and twisting [12]. More complex motions can be achieved by combining multiple fiber arrangements. In addition, as a soft elastomer in which fibers are embedded, the softness and compliance of FRA materials are friendly to human body. Therefore, taking advantage of the motion variance and structure softness, FRAs have the potential to be applied to implement the soft SRLs. Actually, FRAs have been employed in many fields of robotics, such as flexible spine for gecko-inspired wall-climbing robots [13], soft robotic gripper [14], eel-inspired underwater robots [15], and soft robotic sleeve supporting heart function [16]. Applying FRAs into the implementation of the soft SRL is expected to achieve better manipulation and wearing experience. In this article, a soft SRL based on FRAs are designed and implemented. The main contributions of this study are as follows:

(1) A bioinspired soft SRL is designed and implemented, and it is composed of multiple FRAs to mimic the various motions of octopus arms, realizing comfortable wearing experience and flexible manipulation.
(2) Analytic model and finite element model of the FRA are established, based on which, movement trajectory and payload capacity of the SRL are optimized to complete complex operation tasks.
(3) The feasibility and superiority of the proposed SRL system are performed through experiments, and it exhibits comfortable wearing experience, various motion types, accurate motion control and great payload capacity compared with state-of-the-art SRLs.

The remainder of this article are organized as follows: the design and fabrication of the SRL with FRAs are presented in Section 2; the analytic model of each FRA is established in Section 3 and validated with finite element method in Section 4; to complete a prescribed complex trajectory, automatic design of the SRL to get expected movement trajectory and payload capacity is presented in Section 5 and Section 6, respectively; experiments are conducted in Section 7 to validate the developed robot; finally, Section 8 concludes this article.

2 Design and Fabrication

In the applications of traditional rigid SRLs, the operator bodies may be damaged due to their heavy weights and interactive collisions, and the lack of flexible manipulation hinders the operators from completing complex manipulation tasks. To address these problems, a soft SRL is developed in this study. Octopuses give us great inspiration in that they are mollusks with completely soft bodies, and their tentacles can realize various motions, which exactly meet the requirements of the expected SRLs. A unique type of soft tissues structures can be found in octopus arms, termed “muscular hydrostats”, comprising a three-dimensional arrangement of muscle fibers and connective tissue fibers surrounding a central axial nerve cord. Three primary muscle fiber orientations can be observed in the octopus arm musculature, including transverse muscle fibers, longitudinal muscle fibers, and oblique muscle fibers [11]. Biomechanics analysis of the octopus arm suggests that the

contraction of the transverse musculature leads to the elongation of the arm, the longitudinal musculature is responsible for shortening, and the arm bending motion is achieved by contracting the longitudinal muscle fibers on one side of the arm while contracting the transverse muscle fibers, and the torsion can be obtained due to the oblique musculature [17, 18]. Since the muscle fibers are arranged with multiple orientations in the muscular hydrostats, the arm motion can be flexibly controlled in all three dimensions. Moreover, by selectively activating specific muscle fibers, the octopus arm can complete a wide diversity and complexity of movements.

Inspired from the biological phenomenon of octopus arms, a fiber-reinforced mechanism is employed to mimic the function of the muscle fibers in the muscular hydrostats; therefore, fiber-reinforced actuators (FRAs) are developed to reproduce the motion characteristics of octopus tentacles. Basically, the FRA is a hollow silicone tube surrounded by fiber reinforcements, and deformation occurs once it is pressurized by input air. By varying the fiber orientations, different types of deformations can be achieved for the FRA, including axial extension, radial expansion, bending, and twisting, which are identical as the effects of the muscle fibers of octopus arms. In detail, the arrangements of the fiber reinforcements for specific deformation are explained as follows (Fig. 1). **Extension & Expansion:** the fiber reinforcement is wrapped in a symmetrical and double-helix configuration, as the fiber angle (the angle between the horizontal axis and fiber) is increased from zero, radial expansion increases and axial extension decreases until finally, the fibers are axially arranged, the maximal radial expansion occurs without axial extension. **Bending:** the fiber reinforcement is wrapped in a symmetrical and double-helix configuration, where fiber angle is regulated so that the actuator can only expand axially, and a strain-limiting sheet of inextensible material is added to prevent this expansion on one side of actuator. **Twisting:** the fiber reinforcement is wrapped in a single helix configuration, instead of a symmetrical double helical wrapping in the above cases. Furthermore, by combining multiple segments with different fiber configurations in series, more complex and customized actuator behaviors can be observed.

The fabrication of the FRA mainly involves the following procedures. The mold of the FRA is designed with SolidWorks and then manufactured with 3D-printing technology. It should be noticed that ridges are made in the mold, so that thread grooves can be left on the surface of the actuator for further fiber winding. The orientation of ridges should be planned elaborately because it determines the path for winding the fibers and the motion category of the FRA. The mold parts are assembled and firmly held together, with a cylindrical steel rod inserting into indentation at the bottom of the mold. Elastomer (DragonSkin 30 silicone, Smooth-on Inc., USA) is then poured into the mold after removing trapped gas with a vacuum chamber. A 3D-printed cap is placed at the top of the mold to hold the rod and encapsulate the whole mold. The mold with the filled elastomer is left overnight at room temperature to cure. Next day, the steel rod along with the attached actuator main body is removed from the mold. After that, woven fiberglass is attached to the actuator body as a strain limiting layer particularly for the bending FRA, or the elastomer materials for the two halves of the mold possess different stiffnesses. Kevlar fibers are circumferentially wound in a helical pattern around the actuator outside and along the actuator length (exactly along the prescribed thread grooves). At each end of the actuator, the fibers are looped around a few times and tied, and silicon glue (SilPoxy, Smooth-On, Inc., USA) is rubbed on the knot areas to reinforce them. The entire actuator is then encapsulated with a thin silicon layer (DragonSkin 20 silicone, Smooth-on Inc., USA) to anchor all fiber reinforcements. Subsequently, the actuator is removed from the rod using isopropanol as a lubricant. Finally, the both ends of the actuator are capped,

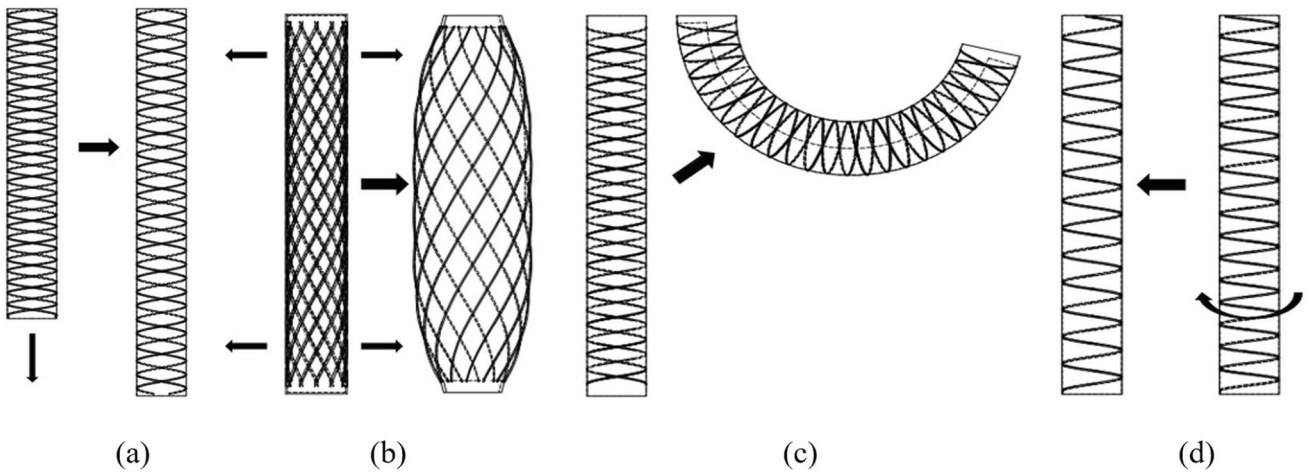

Fig. 1 FRAs with different deformations. **a** Extension; **b** Expansion; **c** Bending; **d** Twisting

and a vented screw is inserted on one end to allow one port for the inflow/outflow of air. Once pressurized air is inflated into the port, the fabricated FRA starts to deform.

Based on the introduction of the FRA, a soft SRL is developed whose design scheme is illustrated in Fig. 2. Connecting multiple FRA modules in series, a highly maneuverable continuum soft SRL is generated. Each FRA module is made by bundles of FRAs in parallel, and the FRAs in one bundle share the same fiber configuration and motion type. A connector is set between two FRA bundles and holds the embedded FRAs tightly. The original length of the whole SRL is designed to approximately match the length of the wearer's arm. At the connector of the distal FRA bundle, a variety of end-effectors can be equipped to manipulate objects, such as suction cup and grasper. The SRL is worn on the human waist with belts, which are made of soft fiber textile materials to ensure comfortable wearing experience. Placing the SRL at the user's waist does not hinder the normal motion of the user's upper and lower limbs, and the SRL is allowed to be align with user body's center of mass, thereby minimizing additional burden exerted on the torso. The contacting area of the belts are designed to be relatively large to reduce the pressure on the human body. The power and control units are placed in the bag on the user's back.

As the proposed SRL have the advantages of comfortable wearing experience, flexible motion trajectory and controllable stiffness, it has great potentials in some particular scenarios. For example, the proposed SRL can be used as the user's both upper and lower extremities. As for daily life, diverse motions for upper extremities, like grabbing and carrying objects and feeding, can be completed by the SRL due to its flexible motion. Utilizing the extending deformation of the FRA, the difference between the upper and lower extremity size can be compensated. The SRL can complete both of stance and swing to assist walking as lower extremity by adjusting its stiffness. Moreover, as for the assembly of aviation equipment, the proposed SRL can provide support and protection for workers who stay in uncomfortable posture like over-head lifting or near-ground crawling, and it can also be used to complete dexterous operations such as guided drilling, auxiliary welding, and tool delivery.

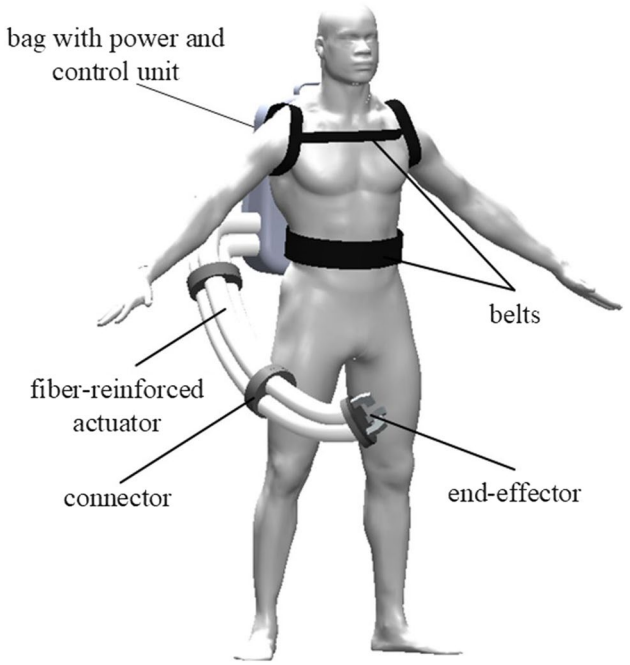

Fig. 2 Design scheme of the SRL with FRAs

3 Analytic Modeling

As described in the previous section, the proposed SRL is composed of multiple FRAs. One FRA can be modeled as a hollow cylinder of isotropic elastomer, surrounded by a thin layer of anisotropic fiber reinforcement. The fibers are tightly embedded in the elastomer, and interaction effects like sliding friction between the elastomer and fiber are neglected. The isotropic cylinder has initial inner radius R_i, outer radius R_o, and initial length L. The initial fiber orientation is determined as $S = (0, \cos\alpha, \sin\alpha)^T$ with α being the fiber angle. Once inflated, the FRA deforms to realize different motions, including extension, expansion, bending, and twisting. Specifically, after deformation, the FRA undergoes a length change $L \to l$, a radius change $R_i \to r_i$ and $R_o \to r_o$, and rotation of one endcap relative to another in radians (twist angle) Φ. Let define the radial, circumferential, and longitudinal coordinates in the reference configuration as R, Θ, and Z; in the pressurized configuration, any point in the FRA is transformed as $R \to r$, $\Theta \to \theta$, and $Z \to z$. The axial stretch is denoted as $\lambda_z = \frac{l}{L}$, so $z = \lambda_z Z$. The radius transformation is formulated as $r^2 - r_i^2 = \lambda_z^{-1}(R^2 - R_i^2)$. The twisting effect is expressed as $\theta = \Theta + Z\frac{\Phi}{L}$. Particularly for the bending deformation, the cross-sections of the cylinder remain planar upon pressurization; therefore, we assume that the radial expansion can be ignored, i.e. $\frac{r}{R} = 1$. Additionally, because the bending actuator has a symmetric arrangement of fibers, no twisting takes place in the bending FRA, i.e. $\Phi = 0$. A deformation gradient [19] can be formulated as follows to describe the parameter change.

$$F = \begin{bmatrix} \frac{\partial r}{\partial R} & \frac{1}{R}\frac{\partial r}{\partial \Theta} & \frac{\partial r}{\partial Z} \\ r\frac{\partial \theta}{\partial R} & \frac{r}{R}\frac{\partial \theta}{\partial \Theta} & r\frac{\partial \theta}{\partial Z} \\ \frac{\partial z}{\partial R} & \frac{1}{R}\frac{\partial z}{\partial \Theta} & \frac{\partial z}{\partial Z} \end{bmatrix} = \begin{bmatrix} \frac{R}{r\lambda_z} & 0 & 0 \\ 0 & \frac{r}{R} & r\frac{\Phi}{L} \\ 0 & 0 & \lambda_z \end{bmatrix} \tag{1}$$

The stress stored inside the FRA is correlated to its strain and material properties, and a strain energy function can be given to reveal the relationship. The FRA mainly comprises two different types of materials, including isotropic elastomer and anisotropic fiber. The elastomer is fabricated

using silicon rubber and can be modeled as an incompressible Neo–Hookean (NH) material [20]. The strain energy for the elastomer is

$$W_{\text{elastomer}} = \frac{\mu_1}{2}(I_1 - 3) \tag{2}$$

where μ_1 is the initial shear modulus of the elastomer, and $I_1 = tr(FF^T)$ with F being the deformation gradient as (1). For the fiber reinforcement, the strain energy is formulated as

$$W_{\text{fiber}} = \frac{\mu_2}{2}(I_4 - 1)^2 \tag{3}$$

where μ_2 denotes the initial shear modulus of the fiber, and $I_4 = s \bullet s$ with $s = FS$. It should be noticed that the above formulation is effective for one set of fibers arranged at the same fiber angle. If multiple sets of fibers are embedded in the FRA, the strain energy needs to be modified as [21]. In this study, only one set of fibers are arranged symmetrically or asymmetrically to realize different motions.

Combining the strain energies of the two components (elastomer and fiber), the total strain energy for the FRA is

$$W = W_{\text{elastomer}} + W_{\text{fiber}} \tag{4}$$

After determining the strain formulation of the FRA, Cauchy stress σ can be used to express the magnitudes of differential stresses in the FRA in cylindrical coordinates. The relationship between the Cauchy stress σ, strain energy W, and deformation F is presented as

$$\sigma = \begin{bmatrix} \sigma_{rr} & \sigma_{r\theta} & \sigma_{rz} \\ \sigma_{\theta r} & \sigma_{\theta\theta} & \sigma_{\theta z} \\ \sigma_{zr} & \sigma_{z\theta} & \sigma_{zz} \end{bmatrix} = \frac{\partial W}{\partial F} F^T - pI \tag{5}$$

where hydrostatic pressure variable p is a Lagrange multiplier arising from the incompressibility of the FRA wall, and I is the identity matrix. The Cauchy stress of the FRA wall is illustrated in Fig. 3.

When a fixed pressure P is input to the FRA, its stretch λ_z, twist Φ, and new radii r_i and r_o are required to quantify the deformation. The radius can be determined by assuming the deformed FRA stresses satisfy a hydrostatic equilibrium; in other words, there is no net stress on an arbitrarily chosen subsection of the FRA wall. The FRA wall needs to be incompressible for holding the equilibrium equations as

$$\begin{aligned} \frac{\partial \sigma_{rr}}{\partial r} + \frac{1}{r}\frac{\partial \sigma_{r\theta}}{\partial \theta} + \frac{\partial \sigma_{rz}}{\partial z} + \frac{1}{r}(\sigma_{rr} - \sigma_{\theta\theta}) = 0 \\ \frac{\partial \sigma_{r\theta}}{\partial r} + \frac{1}{r}\frac{\partial \sigma_{\theta\theta}}{\partial \theta} + \frac{\partial \sigma_{\theta z}}{\partial z} + \frac{2}{r}\sigma_{r\theta} = 0 \\ \frac{\partial \sigma_{rz}}{\partial r} + \frac{1}{r}\frac{\partial \sigma_{\theta z}}{\partial \theta} + \frac{\partial \sigma_{zz}}{\partial z} + \frac{1}{r}\sigma_{rz} = 0 \end{aligned} \tag{6}$$

As we assume that the composite material of the FRA wall is incompressible, the stresses are uniform in z direction and around the FRA wall. Consequently, none of the stresses vary in θ or z direction along the FRA wall, i.e. $\partial\sigma_{r\theta} = \partial\sigma_{rz} = 0$. Because of axial symmetry and uniform stretch, we are primarily interested in the first equation of (6), which is rearranged to induce that $\frac{\partial \sigma_{rr}}{\partial r} = \frac{1}{r}(\sigma_{\theta\theta} - \sigma_{rr})$. The boundary conditions of σ_{rr} are sets as $\sigma_{rr}(r_i) = P$ and $\sigma_{rr}(r_o) = 0$, integrating which induces that

$$P = \int_{r_i}^{r_o} \frac{1}{r}(\sigma_{\theta\theta} - \sigma_{rr})dr = \int_{R_i}^{R_o} \frac{R\lambda_z}{R^2 - R_i^2}(\sigma_{\theta\theta} - \sigma_{rr})dR \tag{7}$$

where $\sigma_{\theta\theta} - \sigma_{rr}$ can be expressed with the FRA dimensions and strain energy as

$$\sigma_{\theta\theta} - \sigma_{rr} = 2\mu_2(I_4 - 1)\left(\frac{r\Phi\sin\alpha}{L} + \frac{r\cos\alpha}{R}\right)^2 - \mu_1\frac{R^2}{r^2\lambda_z^2} \tag{8}$$

Combining (7) and (8), the relationship between the input pressure and deformation parameters, including the radius, length, and twist angle, can be clarified.

Moreover, assuming there is no external axial force or moment exerted on the FRA, the axial load can be obtained as

$$N = P\pi r_i^2 \tag{9}$$

The axial moment for the FRA with extending, expanding and twisting deformation is zero. However, as for the bending FRA, the bend angle of the FRA does not appear in the above Eqs. (7), (8) and (9).

Actually, the FRA bends due to the moment created by the internal pressure acting on the actuator caps M_{cap}, rather than the force exerting on the FRA wall for the extending,

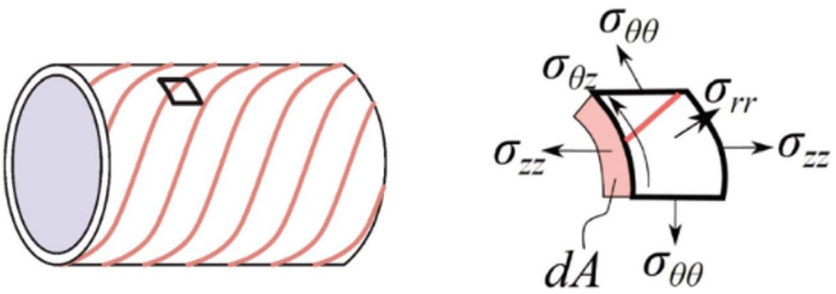

Fig. 3 Differential element of the FRA wall and associated stresses [19]

expanding, and twisting deformation. The internal stretch of the actuator materials results in an opposing bending moment M_{mat}. Hence, at each bending configuration, a torque equilibrium can be reached as $M_{cap} = M_{mat}$.

As presented in Fig. 4, the pressurized force exerted on a micro-area of height h from the bottom edge of the actuator cap, where $h = R_i(1 - \cos\phi)$ with ϕ being the circumferential angle. As the air pressure is exerted on the actuator cap, whose infinitesimal area is defined as $dA = 2R_i \sin\phi dh$, the differential pressure force is calculated as $df = PdA = 2PR_i \sin\phi \mathrm{d}h$, where d$h$ is the differential height. Therefore, the force due to the air pressure acting on actuator cap results in a moment around the bottom edge O is formulated as

$$M_{cap} = 2P\int_0^{2R_i}(h+b)R_i\sin\phi \mathrm{d}h = 2P\int_0^{\pi}[R_i(1-\cos\phi)+b]R_i^2\sin^2\phi \mathrm{d}\phi \tag{10}$$

where b is the initial FRA wall thickness, i.e. $b = R_o - R_i$; dϕ is the differential circumferential angle element.

The resistance moment inside the FRA wall generated by the material can be calculated as

$$M_{mat} = 2\int_0^b\int_0^{\pi}\lambda_z^{-1}\sigma_{zz}\big(R_i+\tau\big)\big(\big(R_i+b\big)-(R_i+\tau)\cos\phi)\big)L\mathrm{d}\phi\mathrm{d}\tau \tag{11}$$

where σ_{zz} is the axial stress of the FRA. As the FRA has a multilayered structure, it is assumed that the effective initial shear modulus of the FRA is denoted as $\overline{\mu}$, which can be obtained through calibration tests [22], and the axial stress can be written as $\sigma_{zz} = \overline{\mu}\lambda_z^2 - \frac{\overline{\mu}}{\lambda_z^2}$. Alternatively, readers can refer to [19] to find the detailed formulation of σ_{zz}. The longitude stretch λ_z can be calculated as

$$\lambda_z = \frac{(L/\varphi)+(b-\tau)}{(L/\varphi)} = \frac{(b-\tau)\varphi}{L} + 1 \tag{12}$$

where φ is the bend angle.

By solving the moment equilibrium equation $M_{cap} = M_{mat}$ with combing (10), (11), and (12), the relationship between the input pressure of the FRA and its bend angle can be obtained as

$$P = \frac{\int_0^b\int_0^{\pi}\lambda_z^{-1}\sigma_{zz}\big(R_i+\tau\big)\big(\big(R_i+b\big)-(R_i+\tau)\cos\phi)\big)L\mathrm{d}\phi\mathrm{d}\tau}{\int_0^{\pi}[R_i(1-\cos\phi)+b]R_i^2\sin^2\phi\mathrm{d}\phi} \tag{13}$$

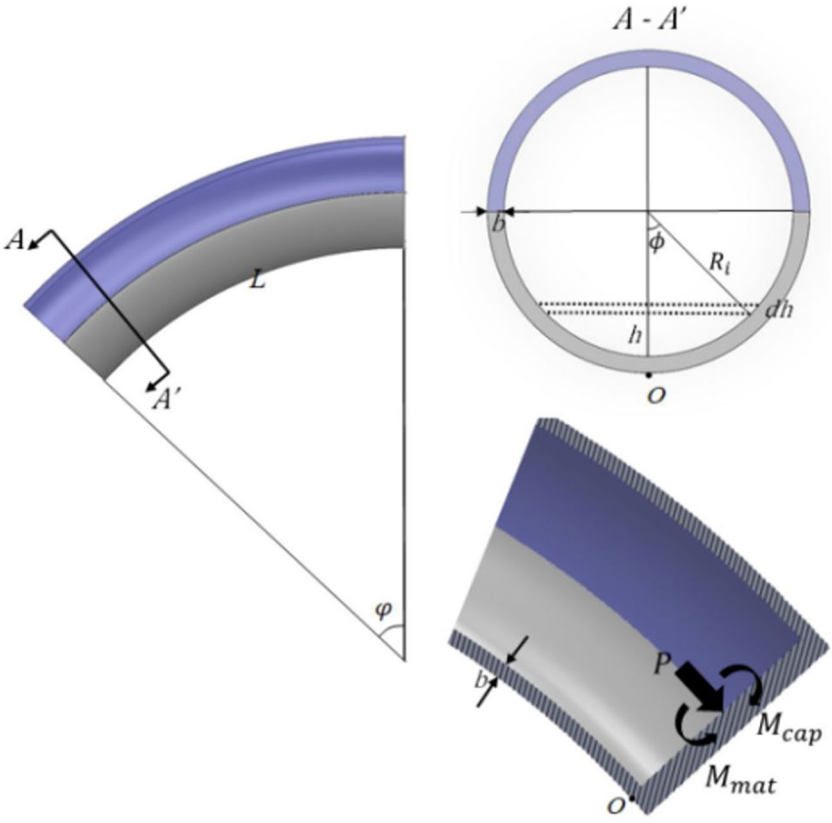

Fig. 4 Cross section of the bending FRA

To this end, the analytic models of a single FRA with different deformations, including extension, expansion, bending, and twisting, are completely established. Once the structure size and input pressure of a FRA are informed, its deformation can be explicitly quantified. Not limited to this, the kinematics of one FRA with complex fiber arrangements or the combination of multiple FRAs (different types of deformations are integrated), is expected to be resolved based on the proposed analytic models.

4 Finite Element Modeling

The aforementioned analytic model quickly generates insights into the geometry deformation behavior of the FRA with responding to the input pressurized air. In order to validate the accuracy of the proposed model, finite element method (FEM) is utilized to describe realistic characteristic of the FRA. By constructing FEM models, intuitive visualization of the FRA deformation can be exhibited. Also, the FEM models can be used to optimize the FRA structure based on the SRL's performance requirement.

The FEM models are constructed and analyzed with ABAQUS/Standard. The elastomers of the FRA are modeled using solid tetrahedral quadratic hybrid elements (Abaqus element type C3D10H). The fiber windings are modeled using quadratic beam elements (Abaqus element type B32), which are connected to the elastomer by tie constraints. Elastomeric samples of the individual materials used to fabricate the actuator are tested according to ASTM D638 (Type IV) at a rate of 500 mm/min for uniaxial tensile strength and material properties. A hyperelastic incompressible Yeoh material model is used to capture the nonlinear material behavior of the SmoothOn DragonSkin material [23]. As Kevlar threads are selected for the fiber reinforcement, they are modeled as a linearly elastic material with the specifications: Young's modulus is 31076 MPa and Poisson's ratio is 0.36. Three identical FRAs are coupled tightly in parallel. After completing the mesh refinement, quasi-static nonlinear simulations are performed, where one end of the actuator is fixed, and a pressure load is applied to the inner surface of the actuator. The deformation of the FRA obtained with the FEM model is illustrated in Fig. 5. In this design of the SRL, the

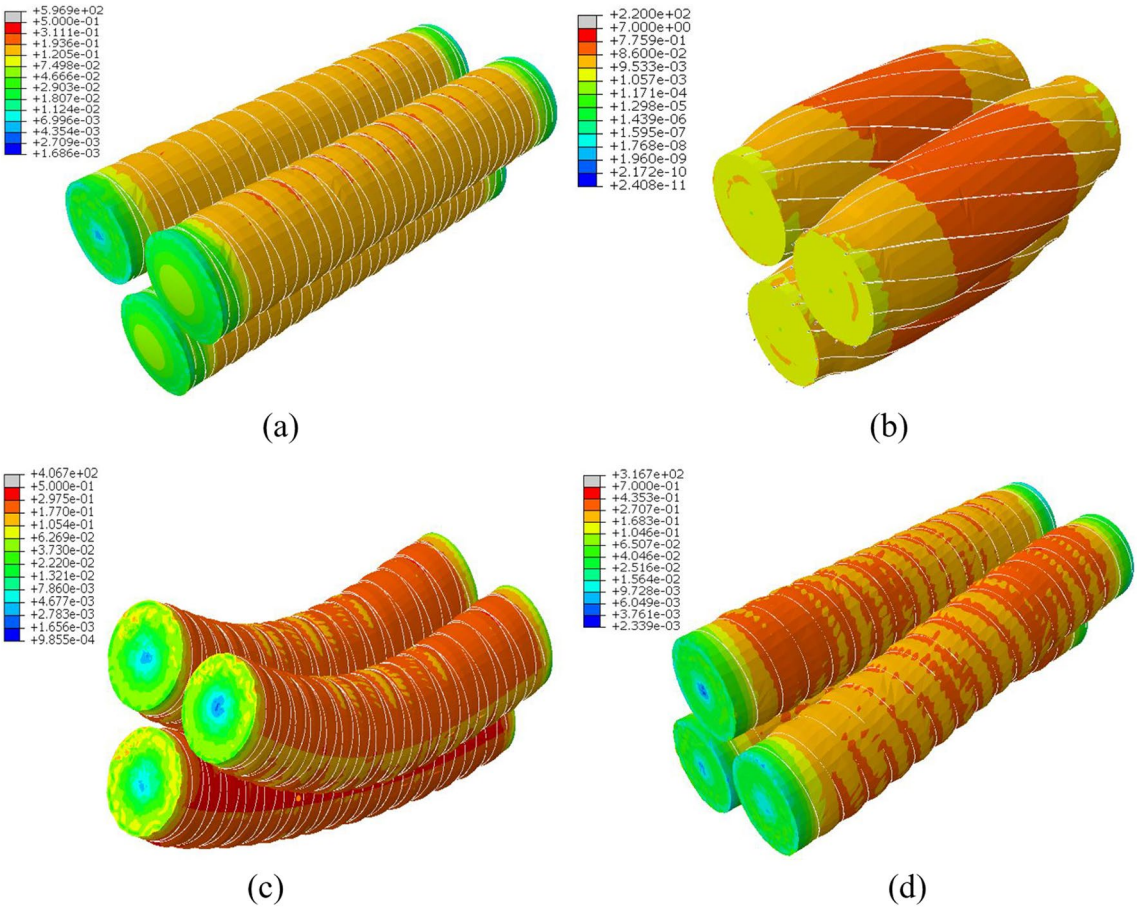

Fig. 5 FEM models of FRA bundles with different motion types. **a** Extension; **b** Expansion; **c** Bending; **d** Twisting

three parallel FRAs in one bundle are independently fixed to the connectors, and the distance between each FRA and connector center is designed to isolate the contact of the three parallel FRAs. Inspired by [26], the nonsmooth contact issue will be studied in our future work to improve the modeling accuracy.

Under different air pressures (P), the deformation parameters for each type of FRA (stretch λ_z for the extending FRA, deformed outer radius r_o for the expanding FRA, bend angle φ for the bending FRA, and twist angle Φ for the twisting FRA) are presented. By comparing the analytic results to FEM results with varying air pressures, great agreement is found in Fig. 6. The discrepancies between theoretical modeling and simulation (less than 3% in each deformation type) are mainly because simplified hyperelastical model for silicon chamber and homogeneous assumptions for restriction layers.

5 Trajectory Optimization

To complete a grasping or delivering task, the SRL is usually required to perform a complex motion with achieving the target and avoiding the obstacles. In most cases, such complex motion can be represented as a combination of extending, expanding, bending and twisting motions. The proposed analytic model can be used to inversely design the SRL with multiple FRA segments that follow a specific trajectory.

Firstly, the objective trajectory is planned and categorized into extending, expanding, bending, and twisting motions manually, and the individual deformation-related geometrical parameters of the related FRAs are extracted in Table 1. A complete motion trajectory can be divided into several sections (or phases) in time series. At the first cycle, the initial geometric, material and loading

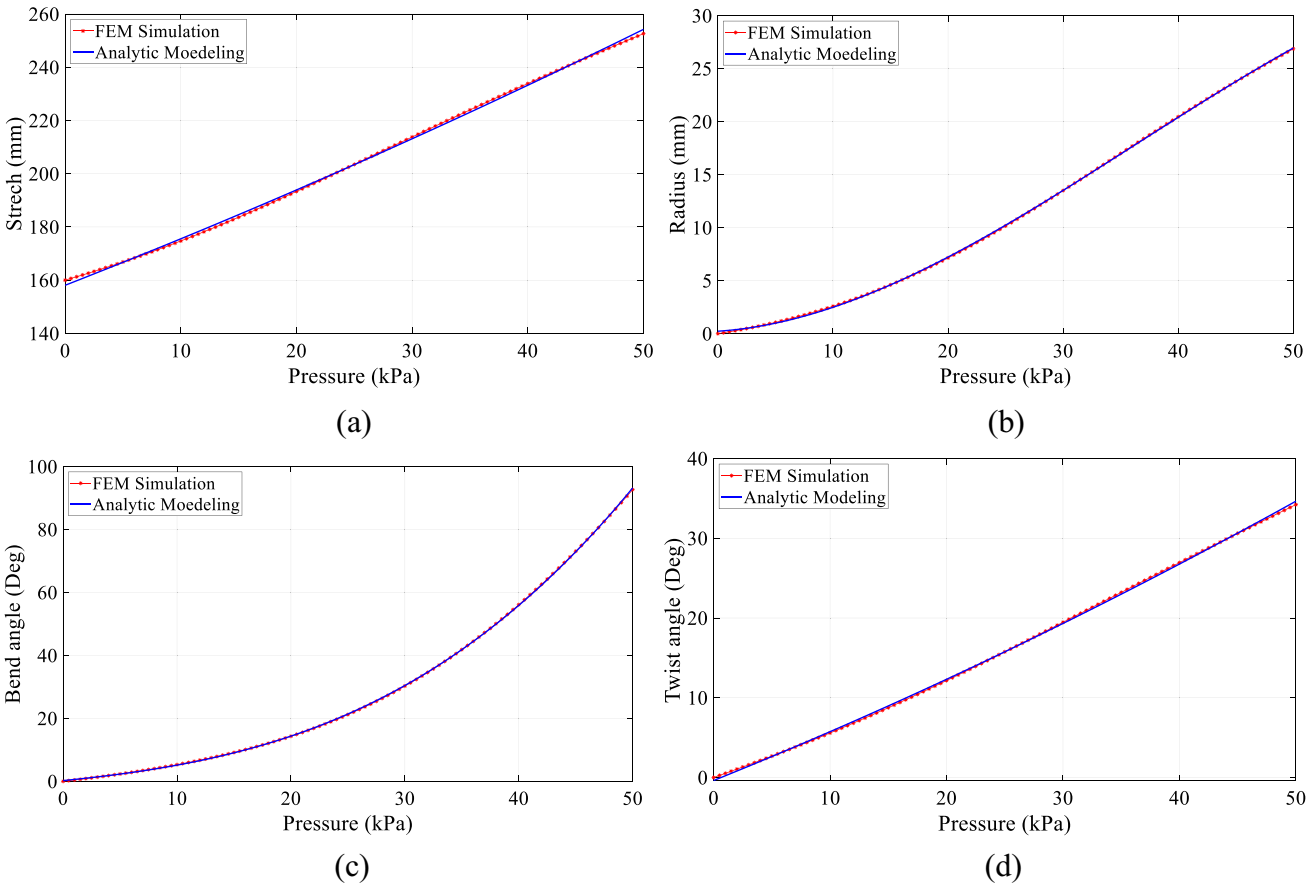

Fig. 6 Comparison between FEM simulation and analytic modeling. **a** Extension; **b** Expansion; **c** Bending; **d** Twisting

Table 1 Specifications of FRAs to realize different motions

FRA motion	Extension	Expansion	Bending	Twisting
Initial geometric parameters	inner radius R_i, outer radius R_o, length L, fiber angle α			
Loading parameters	air pressure P			
Deformed geometric parameters	length l	outer radius r_o	bend angle φ	twist angle Φ

parameters are roughly estimated, and the deformed geometric parameters are calculated using the proposed analytic model. In fact, errors are unavoidable in comparing the deformed shape with the target trajectory. An optimization algorithm is designed to find the optimal design parameters of each FRA to cooperatively replicate the prescribed trajectory.

An objective function is defined as the summation of the shape difference square between the desired trajectory and the theoretically calculated trajectory, such as

$$\mathcal{F} = c_1 \sum_{j=1}^{N_{sec}} \sum_{i=1}^{n_{extend}} \left| l_i - \widehat{l}_i \right|^2 + c_2 \sum_{j=1}^{N_{sec}} \sum_{i=1}^{n_{expand}} \left| r_{o,i} - \widehat{r}_{o,i} \right|^2 + c_3 \sum_{j=1}^{N_{sec}} \sum_{i=1}^{n_{bend}} \left| \varphi_i - \widehat{\varphi}_i \right|^2 + c_4 \sum_{j=1}^{N_{sec}} \sum_{i=1}^{n_{twist}} \left| \Phi_i - \widehat{\Phi}_i \right|^2 \quad (14)$$

where n_{extend}, n_{expand}, n_{bend}, and n_{twist} are the numbers of extending, expanding, bending, and twisting FRA segments, respectively, and N_{sec} is the number of sections. The first term measures the difference between the required ($\widehat{l}_i$) and achieved length (l_i) of the extending FRAs; the second term measures the difference between the required ($\widehat{r}_{o,i}$) and achieved radii ($r_{o,i}$) of the expanding FRAs, and it should be noticed that in the expanding deformation, the increasing cylinder radius might result in the decrease of its length; the third term measures the difference between the required ($\widehat{\varphi}_i$) and achieved bend angles (φ_i) of the bending FRAs; and the fourth term measures the difference between the required ($\widehat{\Phi}_i$) and achieved twist angles (Φ_i) of the twisting FRAs. The parameters c_1, c_2, c_3, and c_4 are the weights that balance the relative importance of each FRA segment with different motion types. The design variables are iteratively updated to minimize the objective function (14) with particle swarm optimization algorithm. When the minimal value of $\mathcal{F}$ is found, the geometric parameters (R_i, R_o, L, α) and air pressure (P) for each FRA segment is optimized. The main objective the trajectory optimization algorithm is to solve the design parameters of the SRL with planning a tailored movement trajectory, and it is a straightforward way to complete the specific task. Usually, the trajectory optimization is treated as the high-level controller, and the low-level controller is also required to track the planned trajectory. The inverse solution of the abovementioned analytic modeling is an effective approach to realize the planned trajectory. In our future work, a high-precision control will also be studied for accurate control performance. In addition to the trajectory optimization for specific tasks, performance-based optimization is also vital. For example, some application scenarios have deformation capacity or workspace requirement, except transferring these performance metrics to the design parameters in Table 1 with the inverse kinematics of the SRL, it is also suggested to utilize the Pontryagin's minimum principle as an alternative for performance-based optimization [27].

6 Payload Optimization

In addition to the deformation trajectory while operating the SRL, the payload capacity should also be taken into account to complete manipulation tasks like pick-and-place and heavy support. The term "payload capacity" refers to the maximum payload that can be carried by the SRL end-effector when the wearer stays in static state, and the FRA is inflated to maintain the SRL in a horizontal position parallel to the ground. We assume that the FRAs are mounted evenly in parallel within one bundle and each has both ends attached to the connector. The end-effector is axially equipped at the distal connector. A position vector $d_i = \left[d_i^X \;\; d_i^Y \;\; d_i^Z \right]^T$ is defined to denote the point where the ith FRA is attached, and a unit vector $a_i = \left[a_i^X \;\; a_i^Y \;\; a_i^Z \right]^T$ is used to express the direction of the associated FRA axis. Let $f_i = \left[F_i^X \;\; F_i^Y \;\; F_i^Z \;\; M_i^X \;\; M_i^Y \;\; M_i^Z \right]^T$ be the force exerted by the ith FRA on the connector, where F_i^X, F_i^Y and F_i^Z are the component of the force along the X-axis, Y-axis and Z-axis of the end-effector frame, respectively, and M_i^X, M_i^Y and M_i^Z are the moment about X-axis, Y-axis and Z-axis of the end-effector frame, respectively (Z-axis is along the central axis of the end-effector) [24]. Therefore, the components of the vector f_i can be computed from the axial force F_i and twisting moment M_i of the ith FRA as

$$\left[F_i^X \;\; F_i^Y \;\; F_i^Z \right]^T = a_i F_i \quad (15)$$

$$\left[M_i^X \;\; M_i^Y \;\; M_i^Z \right]^T = \lfloor d_i \times \rfloor a_i F_i + a_i M_i \quad (16)$$

where $\lfloor d_i \times \rfloor$ is the matrix notation for the cross-product with d_i:

$$\lfloor d_i \times \rfloor = \begin{bmatrix} 0 & -d_i^Z & d_i^Y \\ d_i^Z & 0 & -d_i^X \\ -d_i^Y & d_i^X & 0 \end{bmatrix}$$

The total force f_{total} is the sum of the individual forces of all FRAs, which can be formulated as

$$f_{total} = \sum_{i=1}^{N_{FRA}} f_i = \sum_{i=1}^{N_{FRA}} D_i J_q^T P_i \quad (17)$$

where N_{FRA} is the number of FARs in one bundle; P_i is the input pressure of the ith FRA; J_q^T denotes the relationship between the generalized deformation and input pressure, which has been revealed in (9) and (10); and D_i is matrix that contains the position and orientation vectors as

$$D_i = \begin{bmatrix} [a_i \ 0] \\ [\lfloor d_i \times \rfloor a_i \ 0] + [0 \ a_i] \end{bmatrix}$$

Given a payload task whose desired capacity is f_{des}, and the optimization attributes to shrink the difference between f_{total} and f_{des}. Select the parameters for to be optimized as $\chi = [L_i, R_{ii}, R_{oi}, \alpha_i, P_i, a_i, d_i]^T$ with the subscript i denoting the ith FRA, and the optimization problem is formulated as (18).

$$\text{minimize} J(x) = \sum_{i=1}^{N_{sample}} \frac{(f_{total}^i - f_{des}^i)^2}{N_{sample}} \tag{18}$$

where N_{sample} is the number of samples. The Broyden–Fletcher– Goldfarb–Shanno (BFGS) algorithm together with a penalty barrier algorithm, is employed to find the optimal parameters [25]. The purpose of the payload optimization is to obtain the optimal SRL design parameters χ for a given payload.

7 Experiments

After designing the proposed SRL with FRAs, the robot prototype is manufactured and presented in Fig. 7. The SRL is. The air source is provided by a miniature diaphragm pump (KZP-PF, Kamoer), and the pressurized air is transmitted to the solenoid valves (VQ110U, SMG) through pipes. Each FRA is driven by connecting the vented screw to the pneumatic valves. The pressure is regulated by a microcontroller (Arduino Mega) and potentiometers, and MOSFETs and switches are used to control the opening and closing of the solenoid valves. The miniature diaphragm pumps and valves are selected to ensure the driving speed of the FRAs. Pressure sensors (ASDX, Honeywell) are equipped to provide feedback on the inflow of the FRAs, based on which, the command signals of the microcontroller are adjusted for accurate tracking of the desired pressure. All of the control components are integrated in a breadboard and put into the bag. The overall weight of the SRL limb is 2 kg, not including the drive control units, and the payload-weight ratio of the SRL is approximately 15.

To evaluate the effective workspace, the SRL is initially mounted parallel to the ground, and reflective markers are placed at the proximal and distal ends of the SRL and interconnecting points of each FRA to create virtual bodies. The positions of the markers are captured and recorded using a motion capture system. Individual FRAs are inflated in various configurations using a maximum pressure to illustrate the entire workspace with Monte Carlo method as shown in Fig. 8. The maximal reach, horizontal range, and vertical range of the SRL are 0.81 m, 0.79 m, and 1.20 m, respectively. The SRL is capable of reaching any point inside the

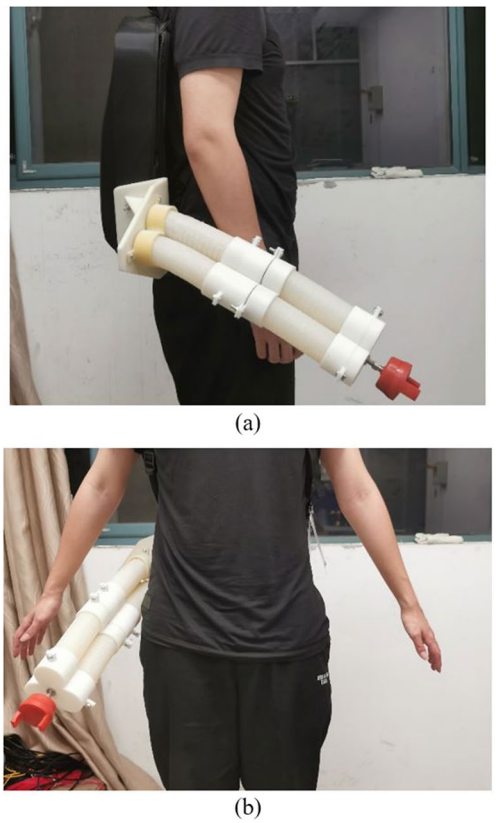

Fig. 7 Prototype of the SRL with FRAs. **a** Side view; **b** Front view

workspace. This workspace provides enough vertical and horizontal range to assist a user in daily life activities.

In order to test the motion controlling performance of the proposed SRL when used in real-life situations, the user is asked to complete a pick-and-place task. Specifically, the target object should be reached by the SRL without touching obstacles. For this experiment, a gripper is equipped at the SRL's end-effector. The experiment is set up for the user to operate the SRL to pick a water bottle (0.6 kg) on one end of a table and move it across and inside a target box ($0.3 \times 0.3 \times 0.2$ m) that is placed 0.4 m away. Four users with no previous experience are timed while performing the task for five times each. The timed results are shown in Table 2, which demonstrate the gradual adoption and improvement in operation of the SRL.

The operation task difficulty is increased by adding obstacles and changing target positions. The positions of the target object and the end-effector of the SRL are captured by using vision trackers to detect the markers on them. The time series data of the coordinates of each marker in three-dimensional space are planned according to the requirement of the task completion and obstacle avoidance, and four sections are selected in this study ($N_{sec} = 4$) to constitute the entire movement trajectory of the SRL. Based on these data, the deformed

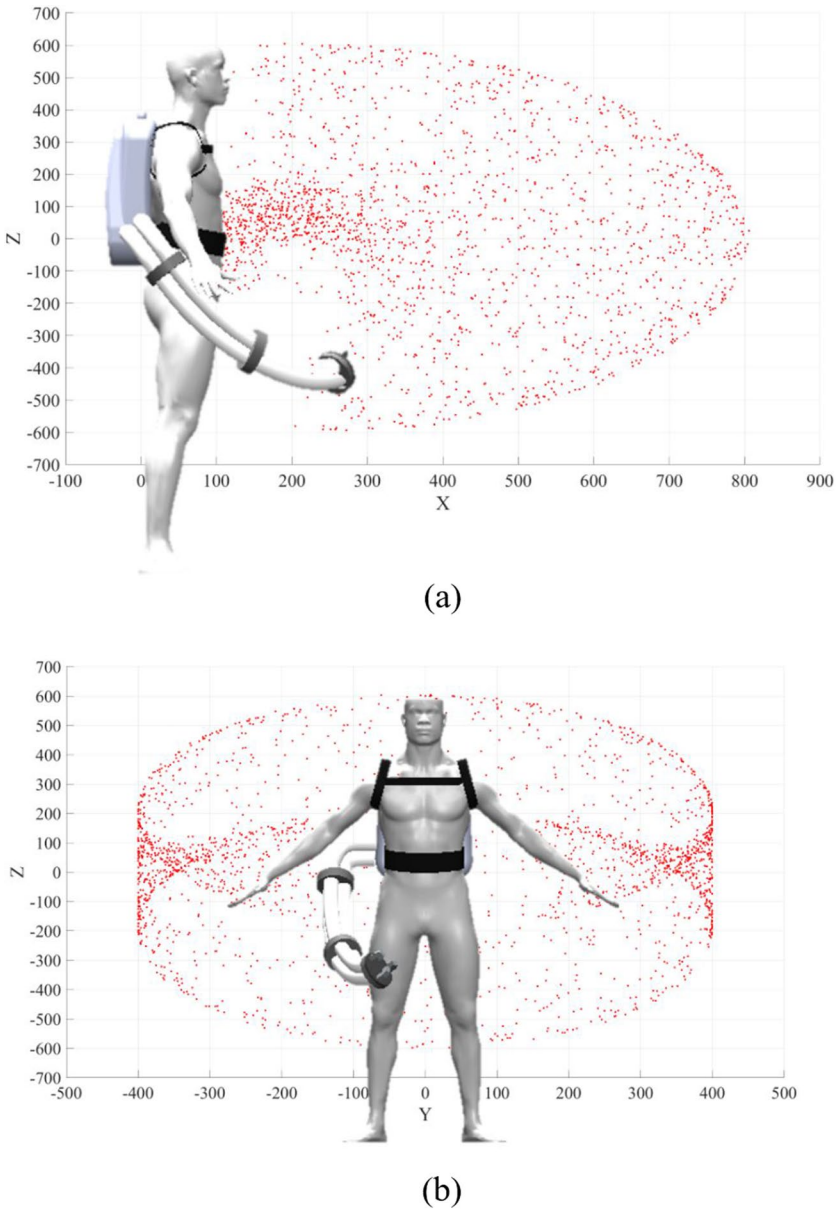

Fig. 8 Illustration of the effective workspace of the SRL. **a** Side view; **b** Front view

Table 2 Pick-and-place time duration

Users	Attempt 1	Attempt 2	Attempt 3	Attempt 4	Attempt 5
1	52.2 s	37.1 s	25.9 s	14.8 s	9.4 s
2	34.3 s	18.9 s	14.3 s	12.9 s	10.6 s
3	37.9 s	32.5 s	26.0 s	20.4 s	16.7 s
4	48.4 s	33.8 s	22.8 s	14.3 s	9.3 s
5	38.5 s	35.3 s	19.2 s	14.5 s	10.4 s

configuration for each FRA are determined by analyzing the inverse kinematics of the SRL, and the initial geometrical parameters for each FRA are optimized through (14). The planned trajectories and the input pressure in each time-phase are depicted in Fig. 9. Three groups of experiments are conducted, where the target and obstacle objects are placed in different locations. It should be noticed that the SRL should be redesigned in each experiment, including the structure sizes of the FRAs and their deformation types and arrangement orders. Each trial is conducted for five times for accuracy. From the experiment results, it can be found that the SRL can successfully achieve the target object, and no collision occurs, even though the number and type of the FRAs are quite different among these three groups of experiments. The deformation types of the FRAs (from near-body to distal) are listed in Table 3, along with the root-mean-square-error (RMSE) and maximal error between the target object and end-effector center positions for the three groups, respectively. Subtle discrepancies exist mostly due to inaccuracies in measuring the actuator motion (for example, misalignment of cameras) as

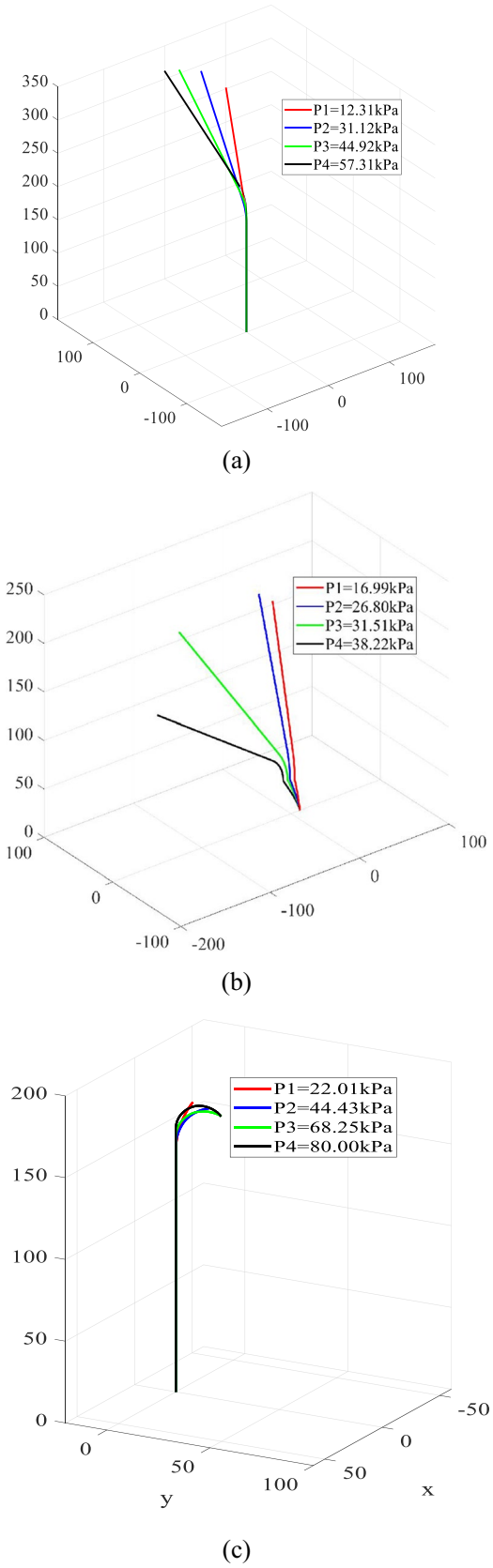

Fig. 9 Trajectory controlling performance. **a** Group A; **b** Group B; **c** Group C

Table 3 Optimal design and control results

Experiment	FRA deformation type			RMSE	Max
Group A	Extension	Bending	Extension	0.34 mm	0.67 mm
Group B	Twisting	Bending	Extension	0.27 mm	0.46 mm
Group C	Extension	Bending	Bending	0.39 mm	0.68 mm

well as defects in actuator fabrication (such as nonuniform wall thickness), but the successful grasping operation is not affected. Therefore, the proposed soft SRL along with its trajectory optimization provides an effective strategy to automatically inverse design the structure based on the specific task requirement, and the input air pressure can be accurately controlled to realize satisfactory movement trajectory tracking performance. Moreover, although other soft SRLs have been developed, their control accuracy is not obviously verified, and the control accuracy of the proposed SRL is more advantageous than current soft SRLs. It should be noticed that the trajectory controlling experiments are conducted under unloaded condition, where the effect of the payload on the trajectory tracking accuracy is not considered herein. The experiments on the trajectory performance with payload will be explained thereafter.

Additionally, experiments are carried out to test the payload capacity of the proposed SRL. Force load cells (LoadStar RAS1-25 lb) and moment load cells (LoadStar RST1-6Nm) are placed on the distal end of the SRL to measure the end-effector forces and moments, respectively. The SRL is fully extended and parallel to the ground with gravitational forces exerting orthogonal to the SRL, and the user operates the SRL to generate forces and moments with counteracting gravity. In this study, three FRAs are mounted evenly in parallel in one bundle, and the distance between each FRA and connector center is set as d_s. All of the three FRAs are orientated to the end-effector central axis, so that

$$
\begin{aligned}
d_1 &= \begin{bmatrix} d_s & 0 & 0 \end{bmatrix}^T \\
d_2 &= \begin{bmatrix} -\frac{d_s}{2} & \frac{\sqrt{3}d_s}{2} & 0 \end{bmatrix}^T \\
d_3 &= \begin{bmatrix} -\frac{d_s}{2} & -\frac{\sqrt{3}d_s}{2} & 0 \end{bmatrix}^T \\
a_1 = a_2 = a_3 &= \begin{bmatrix} 0 & 0 & 1 \end{bmatrix}^T
\end{aligned}
$$

Based on this configuration, the transformation matrices in (17) are written as

$$D_1 = \begin{bmatrix} 0 & 0 & 1 & 0 & -d_s & 0 \\ 0 & 0 & 0 & 0 & 0 & 1 \end{bmatrix}^T$$

$$D_2 = \begin{bmatrix} 0 & 0 & 1 & \frac{\sqrt{3}d_s}{2} & \frac{d_s}{2} & 0 \\ 0 & 0 & 0 & 0 & 0 & 1 \end{bmatrix}^T$$

$$D_3 = \begin{bmatrix} 0 & 0 & 1 & -\frac{\sqrt{3}d_s}{2} & \frac{d_s}{2} & 0 \\ 0 & 0 & 0 & 0 & 0 & 1 \end{bmatrix}^T$$

Once the transformation matrices are prescribed, the resulting force can be calculated through (17). For given movement trajectory tasks, each FRA's length, inner radius, outer radius and fiber angle are determined with (14); afterwards, different payload requirements f_{des} are prescribed, the FRA attachment point positions d_s can be optimized with (18). Increasing the air pressure can test the designed SRL's actual payload. Four groups of the desired payload capacities are tested with load cells, and the SRL's end-effector payload capacities under varying air pressures are depicted in Fig. 10. It can be found from the figures that the resulting force can successfully meet and even exceed the payload requirements, and the proposed payload optimization approach proves effective. By increasing the desired payload and optimally designing the SRL, its maximal payload capacity can be tested, i.e. the payload-weight ratio is over 15. The validation of the SRL trajectory under each desired load condition is conducted based on time duration, the root mean square error (RMSE), and repeatability error of the placing position, as listed in Table 4. As the weight

Table 4 Trajectory performance with payload

Payload	test	Time	RMSE	Repetitive Error
5N	1	7.52 s	0.38 mm	0.53%
	2	8.05 s	0.31 mm	0.48%
	3	6.83 s	0.42 mm	0.57%
10N	1	7.89 s	0.43 mm	0.57%
	2	8.33 s	0.33 mm	0.52%
	3	7.21 s	0.45 mm	0.61%
15N	1	8.23 s	0.47 mm	0.61%
	2	8.59 s	0.36 mm	0.55%
	3	7.68 s	0.49 mm	0.65%
20N	1	8.66 s	0.51 mm	0.64%
	2	8.84 s	0.40 mm	0.59%
	3	8.07 s	0.55 mm	0.69%

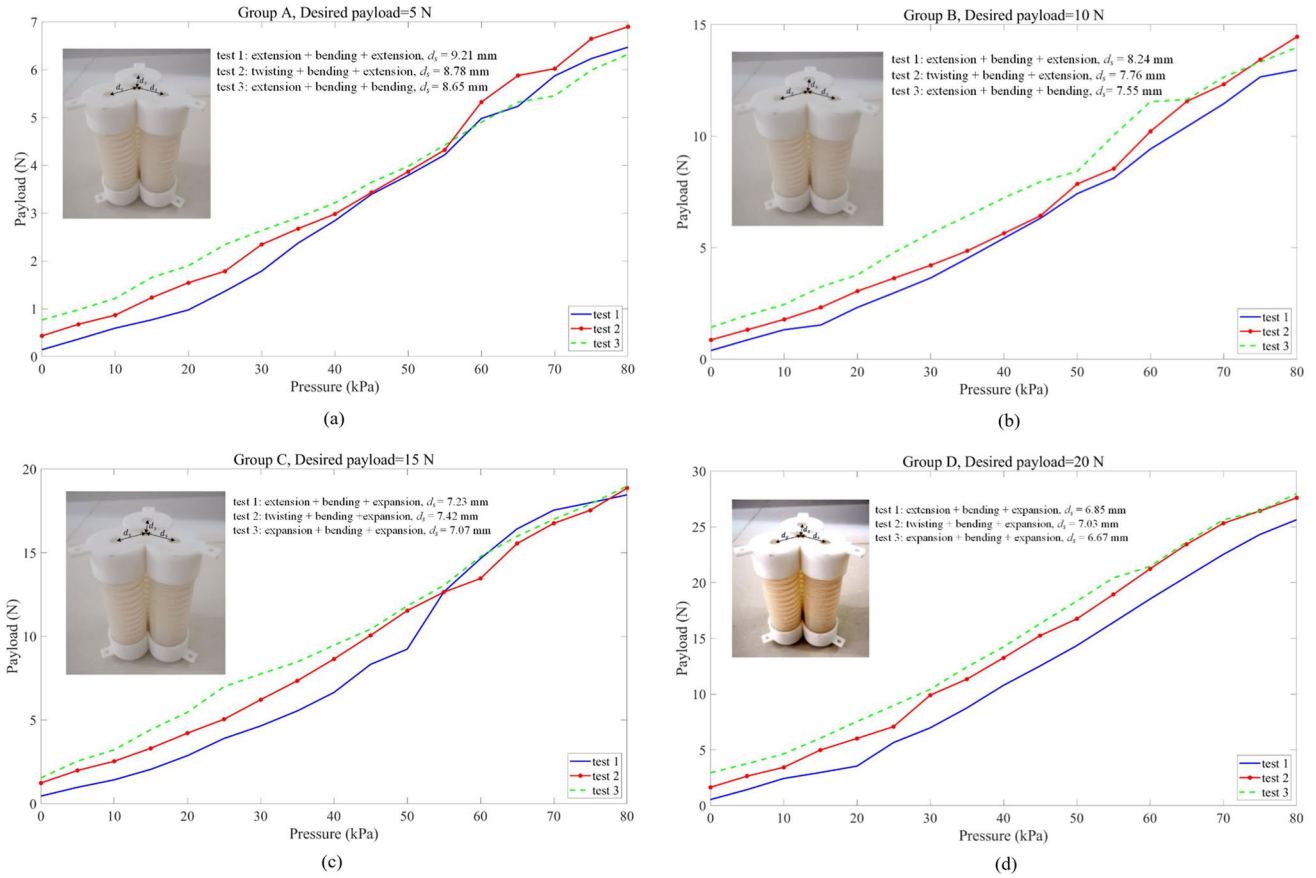

Fig. 10 Payload optimization experiments. **a** Group A; **b** Group B; **c** Group C; **d** Group D

Table 5 Comparison results

	Structure stiffness	Motion type	Workspace	Control accuracy	Payload capacity
Super Limb [3]	Rigid	Rotation	overhead	High	4×
SRL with MRAs [5, 6]	Rigid	Rotation	1.3×1.4×1.5 m	High	0.6×
Soft Poly-Limb [8]	Soft	Extension, bending	0.55×0.69×0.72 m	Not mentioned	2.35×
Fabric soft Poly-Limb [9]	Soft	Bending	0.28×0.695×0.63 m	Not mentioned	10.1×
Proposed SRL	Soft	Extension, expansion, bending, twisting	0.81×0.79×1.2 m	High	15×

of the payload increases, although the time required for each test group of SRL to complete the trajectory gradually increases, the RMSE and repeatability errors remain subtle. Therefore, the proposed SRL is proved to stably and accurately complete the target tasks. Although the designed SRL is able to encounter support tasks in daily life, its payload capacity of the SRL can be further enhanced by adding the number of FRAs in each bundle. To this end, for completing specific operation tasks, including movement trajectory and payload capacity, the SRL can be optimally designed and implemented with the verified approaches, which lays the foundation for future applications of soft SRLs and other soft robotic manipulators. It should be noticed that, by controlling the payload within the capacity range, the trajectory accuracy of the SRL remains stably high. However, when the payload of the SRL reaches its maximum value, the execution accuracy of the predefined trajectory decreases. As the payload continues to increase, the FRAs may fail due to excessive load, resulting in the inability to complete the specified operation or support tasks. Trajectory compensation can be utilized to adapt to the varying payload with ensuring motion accuracy [28].

Moreover, in order to manifest the advantage of the proposed SRL surpassing other state-of-the-art SRLs, discussions on the representative SRLs' characteristics comparison are made. The candidate SRLs contain Super Limb [3], SRL with magnetorheological actuators (MRAs) [5, 6], soft Poly-Limb [8], fabric soft Poly-Limb [9] as well as the proposed one. They are compared in terms of structure stiffness, motion type, workspace, motion control accuracy, and payload capacity (payload-weight ratio). The comparison results are listed in Table 5. As the first two SRLs are made of rigid materials, the merits of light-weight and wearing experience cannot be obviously exhibited. Owing to the application of the FRAs, the proposed SRL have more motion types (including extension, expansion, bending, twisting and their combined motions) than other rigid and soft SRLs, which supports itself in complicated operations. Besides, the proposed SRL has larger workspace than other SRLs except the SRL with MRAs, but much more compliant motion is performed on the proposed SRL. Payload capacity and control accuracy are drawbacks of soft SRLs as usual. In previous soft SRL studies, the movement trajectory control effect has not been emphasized due to the lack of theoretical modeling of the soft materials, not to mention the payload calculation. But as for our proposed SRL, the analytic model and FEM model of the FRAs are constructed, and the trajectory and payload optimization algorithms are proposed to resolve the abovementioned problems. In summary, as we can see from the comparison results, the proposed SRL outperforms other state-of-the-art SRLs to achieve comfortable wearing experience, various motion types, accurate motion control and great payload capacity.

8 Conclusion

In this paper, a soft SRL is designed and implemented. The SRL is composed of multiple FRAs to mimic the various motions of octopus arms, realizing comfortable wearing experience and flexible manipulation. The analytic and finite element models of the FRA are established to reveal the relationship between its deformation and geometrical parameters as well as input air pressures. Based on this, the movement trajectory and payload capacity of the SRL are optimized, so that the SRL can be optimally designed to complete complex operation tasks. Finally, the feasibility and superiority of the proposed SRL system are performed through experiments.

In future work, the human–robot coupling dynamic model will be established to quantitatively describe the interaction mechanism between the proposed SRL and the wearer. Integration of multiple modalities of sensing information, such as posture, electromyography, and electroencephalography signals, can be a potential approach to capture the wearer motion intention. The control of the SRL based on the wearer's motion intention will be studied, so that the SRL's versatility in various operation tasks can be enhanced.

Acknowledgements This work has been supported by the National Natural Science Foundation of China, under Grant 52205018, the Natural Science Foundation of Jiangsu Province under Grant BK20220894, the State Key Laboratory of Robotics and Systems (HIT) under Grant SKLRS-2023-KF-25, the Fundamental Research Funds for the Central

Universities under Grant NS2022048, the Nanjing Overseas Scholars Science and Technology Innovation Project under Grant YQR22044, and the Scientific Research Foundation of Nanjing University of Aeronautics and Astronautics under Grant YAH21004.

Authors' Contributions All authors contributed to the study, conception, and design. Experiments were conducted by Tianyi Zhang and Mengcheng Zhao. Algorithm coding and data processing were performed by Kaizhen Huang. Supervision and funding management were performed by Jiajun Xu, Xuyan Hou and Youfu Li. The first draft of the manuscript was written by Jiajun Xu. All authors read and approved the final manuscript.

Funding This work has been supported by the National Natural Science Foundation of China under Grant 52205018, the Natural Science Foundation of Jiangsu Province under Grant BK20220894, the State Key Laboratory of Robotics and Systems (HIT) under Grant SKLRS-2023-KF-25, the State Key Laboratory of Robotics under Grant 2023-O16, the Fundamental Research Funds for the Central Universities under Grant NS2022048, the Nanjing Overseas Scholars Science and Technology Innovation Project under Grant YQR22044, and the Scientific Research Foundation of Nanjing University of Aeronautics and Astronautics under Grant YAH21004.

Data availability Not applicable.

Code availability Not applicable.

Declarations

Conflicts of interest/ Competing interests. No conflicts of interest.

Ethics approval Not applicable.

Consent to participate Not applicable.

Consent for publication Not applicable.

References

1. Tong, Y., Liu, J.: Review of research and development of supernumerary robotic limbs. IEEE/CAA J Automatica Sinica **8**(5), 929–952 (2021)
2. Parietti, F., & Asada, H. H. (2014). Supernumerary robotic limbs for aircraft fuselage assembly: body stabilization and guidance by bracing. In 2014 IEEE International Conference on Robotics and Automation (ICRA) (pp. 1176–1183).
3. Luo, J., Gong, Z., Su, Y., Ruan, L., Zhao, Y., Asada, H.H., Fu, C.: Modeling and balance control of supernumerary robotic limb for overhead tasks. IEEE Robot Autom Lett **6**(2), 4125–4132 (2021)
4. Daniel, P.H., Fu, C., Asada, H.H.: Musculoskeletal load analysis for the design and control of a wearable robot bracing the human body while crawling on a floor. IEEE Access **10**, 6814–6829 (2021)
5. Khazoom, C., Caillouette, P., Girard, A., Plante, J.S.: A supernumerary robotic leg powered by magnetorheological actuators to assist human locomotion. IEEE Robot Autom Lett **5**(4), 5143–5150 (2020)
6. Véronneau, C., Denis, J., Lebel, L.P., Denninger, M., Blanchard, V., Girard, A., Plante, J.S.: Multifunctional remotely actuated 3-dof supernumerary robotic arm based on magnetorheological clutches and hydrostatic transmission lines. IEEE Robot Autom Lett **5**(2), 2546–2553 (2020)
7. Polygerinos, P., Correll, N., Morin, S.A., Mosadegh, B., Onal, C.D., Petersen, K., Shepherd, R.F.: Soft robotics: Review of fluid-driven intrinsically soft devices; manufacturing, sensing, control, and applications in human-robot interaction. Adv Eng Mater. **19**(12), 1700016 (2017)
8. Nguyen, P.H., Sparks, C., Nuthi, S.G., Vale, N.M., Polygerinos, P.: Soft poly-limbs: Toward a new paradigm of mobile manipulation for daily living tasks. Soft Rob. **6**(1), 38–53 (2019)
9. Nguyen, P. H., Mohd, I. I., Sparks, C., Arellano, F. L., Zhang, W., & Polygerinos, P. (2019). Fabric soft poly-limbs for physical assistance of daily living tasks. In 2019 International Conference on Robotics and Automation (ICRA) (pp. 8429–8435).
10. Liang, X., Cheong, H., Sun, Y., Guo, J., Chui, C.K., Yeow, C.H.: Design, characterization, and implementation of a two-DOF fabric-based soft robotic arm. IEEE Robot Autom Lett **3**(3), 2702–2709 (2018)
11. Kier, W.M., Stella, M.P.: The arrangement and function of octopus arm musculature and connective tissue. J Morphol. **268**(10), 831–843 (2007)
12. Connolly, F., Polygerinos, P., Walsh, C.J., Bertoldi, K.: Mechanical programming of soft actuators by varying fiber angle. Soft Rob. **2**(1), 26–32 (2015)
13. Chen, G., Lin, T., Lodewijks, G., Ji, A.: Design of an active flexible spine for wall climbing robot using pneumatic soft actuators. J. Bionic Eng. **20**(2), 530–542 (2023)
14. Wei, S., Wang, T., Gu, G.: Design of a soft pneumatic robotic gripper based on fiber-reinforced actuator. J Mech Eng. **53**(13), 29–38 (2017)
15. Feng, H., Sun, Y., Todd, P.A., Lee, H.P.: Body wave generation for anguilliform locomotion using a fiber-reinforced soft fluidic elastomer actuator array toward the development of the eel-inspired underwater soft robot. Soft Rob. **7**(2), 233–250 (2020)
16. Roche, E. T., Horvath, M. A., Wamala, I., Alazmani, A., Song, S. E., Whyte, W., ... & Walsh, C. J. (2017). Soft robotic sleeve supports heart function. Sci Translational Med., 9(373), eaaf3925. https://doi.org/10.1126/scitranslmed.aaf3925.
17. Ahmadi, A., Asgari, M.: Novel bio-inspired variable stiffness soft actuator via fiber-reinforced dielectric elastomer, inspired by Octopus bimaculoides. Intel Serv Robot. **14**(5), 691–705 (2021)
18. Laschi, C., Mazzolai, B., Mattoli, V., Cianchetti, M., Dario, P.: Design of a biomimetic robotic octopus arm. Bioinspir Biomim. **4**(1), 015006 (2009)
19. Sedal, A., Bruder, D., Bishop-Moser, J., Vasudevan, R., Kota, S.: A continuum model for fiber-reinforced soft robot actuators. J. Mech. Robot. **10**(2), 024501 (2018)
20. Ogden, R. W. (1997). Non-linear elastic deformations. Courier Corporation.
21. Connolly, F., Walsh, C.J., Bertoldi, K.: Automatic design of fiber-reinforced soft actuators for trajectory matching. Proc Natl Acad Sci. **114**(1), 51–56 (2017)

22. Polygerinos, P., Wang, Z., Overvelde, J.T., Galloway, K.C., Wood, R.J., Bertoldi, K., Walsh, C.J.: Modeling of soft fiber-reinforced bending actuators. IEEE Trans Rob. **31**(3), 778–789 (2015)
23. Yeoh, O.H.: Some forms of the strain energy function for rubber. Rubber Chem Technol. **66**(5), 754–771 (1993)
24. Bruder, D., Sedal, A., Vasudevan, R., Remy, C.D.: Force generation by parallel combinations of fiber-reinforced fluid-driven actuators. IEEE Robot Autom Lett. **3**(4), 3999–4006 (2018)
25. Zhao, W.: A Broyden–Fletcher–Goldfarb–Shanno algorithm for reliability-based design optimization. Appl Math Model. **92**, 447–465 (2021)
26. Ningning, S., Mengru, Z., Fei, L., Ziyun, K., Jian, Z., Haijun, P.: Dynamic research on winding and capturing of tensegrity flexible manipulator. Mech Mach Theory **193**, 105554 (2023)
27. Evers, A.: Sensitivity analysis in dynamic optimization. J. Optim. Theory Appl. **32**(1), 17–37 (1980)
28. AlAttar, A., Hmida, I. B., Renda, F., & Kormushev, P. (2023). Kinematic-model-free tip position control of reconfigurable and growing soft continuum robots. IEEE Int Conf Soft Robot., 1–7.

Jiajun Xu was born in Taizhou City, Jiangsu Province, China in 1993. He received the B.S. degree in mechanical engineering from Hefei University of Technology in 2016 and the Ph.D. degree from University of Science and Technology of China and City University of Hong Kong concurrently in 2021. After that, he joined Nanjing University of Aeronautics and Astronautics and is currently an assistant professor in College of Mechanical and Electrical Engineering. His research interest includes wearable robotics, medical robotics, biomimetic robotics, human-robot interaction control, and machine learning.

Tianyi Zhang was born in Benxi City, China, in 2000. He received the B.S. degree from Nanjing University of Aeronautics and Astronautics (NUAA), Nanjing, China, in 2022, and after that he stay at NUAA to continue to study for the master's degree with the College of Mechanical and Electrical Engineering. His research interests include supernumerary robotic limbs, human-robot interaction control, wearable robotics and rehabilitation robotics.

Kaizhen Huang was born in Ji'an City, Jiangxi Province, China, in 2000. He received the B.S. degree from the Nanjing Agricultural University, Nanjing, China, in 2022, majoring in mechanical engineering. He is currently working toward the Master's degree from Nanjing University of Aeronautics and Astronautics, majoring in mechanical and electronic engineering. His major research interests include soft exosuit, variable stiffness control, human intention detection, and human-robot interaction.

Mengcheng Zhao was born in Chongqing city, China, in 2001. He received the B.S. degree from the Chongqing University of Posts and Telecommunications, China, in 2023. At present, He is currently pursuing the master's degree of mechanical engineering at Nanjing University of Aeronautics and Astronautics, Nanjing, China. His major research interests include soft robotics, biomimetic robotics, and physical human-robot interaction.

Xuyan Hou received his M.D. and Ph.D. from the Harbin Institute of Technology in 2004 and 2009, respectively. He joined the Harbin Institute of Technology in 2009 and is currently a professor. His major research is spatial intelligent bionic institutions. He is a young scholar of the Ministry of Education's "Yangtze River Scholars Award Program". As the first author and corresponding author (including co-authors), he has published more than 50 SCI indexed papers in top international journals such as "Nature Communications", and edited and published 2 academic monographs. He served as a young editorial board member of "Journal of Bionic Engineering" and a reviewer for "Nature Communications" and other journals.

Youfu Li received the Ph.D. from the Department of Engineering Science, University of Oxford, U.K., in 1993. He joined the City University of Hong Kong in 1995 and is currently a professor. His research includes robot sensing, robot vision, and visual tracking. Dr. Li has served as an Associate Editor for IEEE Transactions on Automation Science and Engineering and IEEE Robotics and Automation Magazine, an Editor for CEB and IEEE International Conference on Robotics and Automation, and a Guest Editor for IEEE RAM.